

# INTEGRATED RANGE CAMERA CALIBRATION USING IMAGE SEQUENCES FROM HAND-HELD OPERATION

Wilfried Karel

Christian Doppler Laboratory for Spatial Data from Laser Scanning and Remote Sensing at the Institute of Photogrammetry and Remote Sensing, Vienna University of Technology Gusshausstrasse 27-29 / E122, 1040 Vienna, Austria - wk@ipf.tuwien.ac.at

**KEY WORDS:** Imaging Systems, 3D Sensors, Calibration, Close Range Photogrammetry, Video Camera, Machine Vision

## ABSTRACT:

This article concentrates on the integrated self-calibration of both the interior orientation and the distance measurement system of a time-of-flight range camera that employs amplitude-modulated, continuous-wave, near-infrared light (photonic mixer device - PMD). In contrast to other approaches that conduct specialized experiments for the investigation of individual, potential distortion factors, in the presented approach all calculations are based on the same data set being captured under near-real-world conditions, guided by hand and without auxiliary devices serving as high-order reference. Flat, circular targets stuck on a planar whiteboard and with known positions are automatically tracked throughout the amplitude layer of long image sequences. These image observations are introduced into a bundle block adjustment, which on the one hand results in the determination of the camera's interior orientation and its temporal variation. On the other hand, the reconstructed exterior orientations and the known planarity of the imaged board allow for the derivation of reference values of the actual distance observations. These deviations are checked on relations with the reference distance itself, the observed signal amplitude, the integration time, the angle of incidence, and with both the position in the field of view and in object space. Eased by the automatic reconstruction of the camera's trajectory and attitude, several thousand frames are processed, leading to comprehensive statistics.

## 1. INTRODUCTION

Range Imaging (RIM) denotes the capture of distances at the pixels of a focal plane array using simultaneous time-of-flight measurements. Thereby, the round-trip time of the emitted signal and hence the object distance may be determined in various ways. Currently, alternatives employing nanosecond Laser pulses are highly investigated. So-called Flash LADARs or Laser Radars utilize avalanche photo diodes (APD) for photon detection, eventually supported by photo cathodes for signal amplification (Stettner et al., 2004), and may facilitate maximum observable distances of up to a kilometre. Another technique, called Time-Correlated Single Photon Counting, employs the most sensitive single photon avalanche diodes (SPAD) as detectors (Aull et al., 2002, Niclass et al., 2007, Pancheri et al., 2007, Wallace et al., 2001), minimizing the requirements on the illumination power. In Multiple Double Short Time Integration (MDSI), different fractions of the echo energy are captured in consecutive images by varying the shutter speed and using conventional chips that integrate the irradiance (Mengel et al., 2001, Elkhaili et al., 2004). The requirements for nanosecond Laser pulses or high-speed shutters and the integration of highly precise, miniaturized timing circuitry however boost the complexity and costs of all these systems.

Photonic mixer devices (PMD, lock-in pixels) employ incoherent, near-infrared, amplitude-modulated, continuous wave (AM-CW) light and determine the signal phase shift and hence the object distance by mixing the emitted with the returned signal at every pixel (Spirig et al., 1997, Lange et al., 1999). As on the one hand, the illumination unit of PMD close-range cameras may be realized with low-cost LED arrays, and on the other hand, the operation point of the system is limited to the single frequency of modulation, implying that the demands

on the electronic components are lower (Büttgen et al., 2005), the purchase costs are comparatively low, lying in the range of professional SLR cameras.

The present article concentrates on this latter technique, implemented in the Swissranger™ SR-3000 by MESA Imaging AG. This instrument samples the correlation function of the emitted and returned signal one after another at every quadrant of the modulation period. It features a sensor resolution of 144×176 pixels, a fix-focus lens, range and amplitude data encoded with 16 bit, an overall ranging precision of a few centimetres, and a maximum range of 7.5m when using the default modulation frequency. As other PMD cameras, its ranging system suffers from large systematic distortions reaching decimetres, why comprehensive calibration methods are needed in order to harness the potentials of RIM for geometry- and quality-oriented realms.

### 1.1 Related Work

For the correct reconstruction of the object space imaged by a range camera, knowledge of its interior orientation is an essential prerequisite in combination with undistorted range observations. Westfeld (2007) determines the intrinsic projection parameters by application of conventional photogrammetric techniques to amplitude images, and reports an unstable position of the principal point. Having calibrated the camera optics, Lindner and Kolb (2006) gather range images at known distances from a planar target and experience the deviations of the range measurements as being partly of periodic nature. Steitz and Pannekamp (2005) report influences of the angle of incidence and the surface type on the range observations. Kahlmann *et al.* (2006) perform elaborate laboratory experiments and also reveal the partly cyclic non-linearities of the distance observations. Additionally,

dependencies of the range measurements on the operating and the integration time are reported, and impacts of the external temperature have been published (Kahlmann, 2007).

Only recently, Mure-Dubois and Hügli (2007) have reported on secondary reflections occurring between the lens or filter and the sensor of PMD cameras, which may yield heavy distortions of range observations hitherto disregarded by the PMD calibration community. This way calling extensive experiments and analyses into question again, one may become aware of the circumstance that the set of major PMD error sources has not been isolated yet. Aiming at comprehensive calibrations, it thus may be beneficial to investigate real-world data, possibly discovering important influences this way. Karel *et al.* (2007) capture scenes that feature planar faces, detect and reconstruct them based on the range observations, and investigate the ranging precision based on the deviations. Clear dependencies of the ranging precision on the true distance, the signal intensity and the position in the field of view are found. Lindner and Kolb (2007) use a PMD camera in combination with a conventional RGB camera, mounted on a common, solid rig. The authors observe interdependent influences on the range observations of the signal amplitude, the true distance, and the integration time.

## 1.2 Objective

PMD cameras feature sensor resolutions of a hundred by a hundred pixels only, but offer frame rates exceeding 20Hz. While other PMD calibration approaches base on the low-resolution still images, the presented work tries to capitalize the high temporal data resolution by evaluating image sequences. Following from the statements above, the employed data should furthermore be captured under conditions close to those of real-world applications, hence being affected by similar distortions and featuring some amount of randomness concerning the capture parameters. The quantification of individual error sources may be more complicated this way than it is under laboratory conditions. However, concerning the instrument's applicability, the enhancement of its overall performance is most interesting, not the quantification of specific phenomena. Moreover, a readily neglected point is the fact that even sophisticated experiments may not be able to isolate the influence of certain error factors either, e.g. varying the object distance while maintaining the amplitude level is hard to achieve. This makes the free choice of measurement conditions in the laboratory somewhat irrelevant. As stated above, the interior orientation has shown to be unstable, while the temporal stability of the factors distorting the range observations has not been proved yet. This again calls for self-instead of laboratory calibrations. In order to make it useful for a broader public, the strategy should furthermore avoid the requirement for auxiliary high-order reference devices.

In this work, flat, circular targets stuck on a planar whiteboard at known positions are imaged by the range camera and detected in the amplitude images, allowing for the spatial resection of the camera pose. The object distance of each pixel footprint can thus be computed and compared to the actual range observation. The camera is guided by hand, this way introducing some amount of randomness. As the frame rate is rather high compared to the slow hand movements, the targets can be tracked automatically, allowing for the capture of huge data sets and the derivation of comprehensive statistics.

With the approach being applied for the first time, the

measurement conditions are slightly simplified for now and some potential error sources probably avoided. Thus, having activated the camera, the warm-up period is awaited, the device is operated under constant temperature conditions, and the target plane is chosen to reflect homogeneously. The different reflectivity on areas covered by the targets heavily affects the distance measurements, why these image regions are excluded from the evaluation of distance deviations. However, three concerns remain in conjunction with the approach. Although the influence of scattering is said to be rather low for surfaces of similar object distance, the affected area around the targets shall be investigated beforehand. Kahlmann (2007) reports on erratic fluctuations of the distance measurement system, possibly originating from the cooling system. At least the range of fluctuations shall be determined in advance. Finally, the camera's movements during exposure certainly introduce some motion blur in the data. While this latter issue has not been investigated further so far, respective experiments concerning the first two are described in the following section.

## 2. PRELIMINARY CHECKS

### 2.1 Temporal Stability after Warm-Up

This first preliminary check shall demonstrate that the camera features an acceptable level of measurement stability over time. For that purpose, both the camera's orientation and the imaged object space keep unchanged during half an hour, while constantly gathering data. Figure 1 shows the arithmetic means of the amplitudes and distances captured in each frame of the sequence. With high peaks in the power spectrum around 22 frames per cycle, the Fourier analyses of the two signals confirm the visually noticeable periodicity of both signals. Most important here, the distance varies within around 3mm, while the variation of the amplitude amounts to less than a thousandth of the encoding depth. Compared to the maximum range and the ranging precision, the temporal variation is considered being negligible concerning the purpose of this work.

### 2.2 Scattering

Considering the possibly wide-area impact of the scattering phenomenon reported in literature, a corresponding test seems to be vital that ensures the independence of range observations from the distance between the observing pixels and the targets' images. As the effect needs merely be detected and not quantified, its reported slight anisotropy is neglected and a radial impact is investigated. Again, the camera is mounted on a tripod and directed towards a static, planar surface. Having captured dozens of images of the plane, one of the target markers later on used for the calibration test fields is brought into the field of view, dangling by a thread that is guided from above and outside the imaged area, closely in front of the plane. This way, the target is smoothly directed through the whole image. Having finished, further images of the static scene are gathered. The arithmetic mean of the images captured before and after the appearance of the target serves as background image. In the other images, the target is detected and the corresponding image areas together with those covered by the thread are excluded from further evaluation, making use of the knowledge of the approximate image scale. The background image is subtracted from the masked images, and the remaining range residuals are grouped and averaged by the distance between each observing pixel and the instantaneous position of the target in the image plane. Figure 2 presents the resulting

mean differences from the background image. This test has been carried out for object distances ranging from 60cm to 260cm and integration times from  $4 \times 2.2\text{ms}$  to  $4 \times 20.2\text{ms}$ . However, none of them resulted in statistically significant deviations from zero, why the effect of scattering is assumed to be negligible in the following. By the way, the same has been found to hold for the amplitude observations.

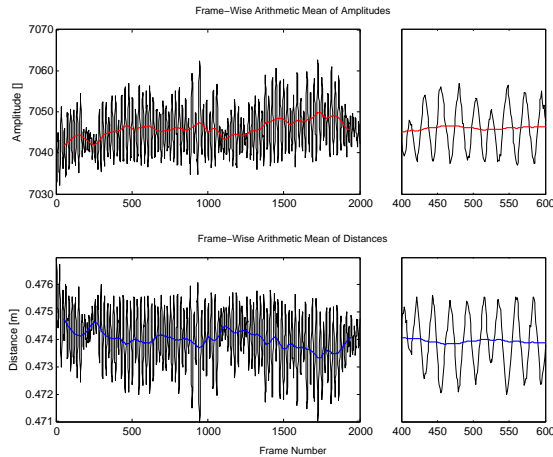


Figure 1. Frame-wise arithmetic mean of amplitudes (top) and distances (bottom). Enlarged details pointing out the periodicity of the signals (right).

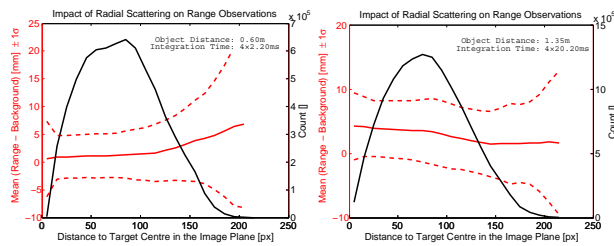


Figure 2. Arithmetic mean of the background subtracted range observations, depending on the distance between the observing pixels and the instantaneous position of the imaged target (red, solid), surrounded by its standard deviation (red, dashed), and corresponding observation counts (black). The results are shown for object distances and integration times of 0.6m/ $4 \times 2.2\text{ms}$  (left), and 1.35m/ $4 \times 20.2\text{ms}$  (right).

### 3. ROBUST TARGET TRACKING

For the purpose of gathering large amounts of reference data, the coordinates of the target centres pictured in the amplitude images must be determined automatically. As the calibration data shall cover both a wide range of integration times and object distances, low-amplitude data is inevitable. In addition to the resulting high noise levels, the employed calculus must cope with repetitive image structures (cf. section 4.1). Because of both the vignetting of the objective and the (roughly) radially decreasing power of illumination, the amplitude generally decreases towards the image borders. As no image preprocessing shall be applied, the algorithm must manage hugely imaged targets featuring inhomogeneous amplitude values.

Among other, more common target centroiding methods, the stepwise adjustment of the target model described in (Otepka, 2004) demonstrates best performance concerning the shortcomings of the amplitude data in use. Furthermore, this procedure yields additional results that can be used for plausibility checks and weighting in subsequent adjustments.

The tracking of targets as implemented for this work is based on the detection of potential target areas by morphological image processing, adjustments of the aforementioned target model, the matching of the resulting target centres with their projection from the test field (based on the recent exterior orientation, nearest neighbours and considering the planar shift from the recent image found by correlation), and the subsequent adjustment of the camera's current exterior orientation using L1- and L2-norms. Furthermore, some plausibility checks are performed.

### 4. CALIBRATION

Sensors of digital amateur cameras are reported to be rather loosely coupled to their casing, resulting in an unstable interior orientation possibly sensitive to agitation or somehow following gravity. In order to avoid displacements of the sensor with respect to the projection centre during data capture, it is thought to be advantageous to keep the optical axis directing either up- or downwards and to avoid rotations about it. Lacking a convex 3-D surface, the calibration of the ranging system needs to be realized on a 2-D test field in order to avoid multipath effects in object space. The camera calibration described in this work bases on known control point positions, but treats both the camera's interior and exterior orientations as unknowns. Using a planar field of control points, unknown interior and exterior orientations are however prone to be considerably correlated to each other, especially if images with different rotations about the optical axis are absent. For the purpose of a more thorough investigation of the interior orientation, thus a calibration on a 3-D test field is conducted, which exclusively uses the amplitude images (cf. subsection 4.1). The calibration integrating the range measurements however uses a 2-D field (cf. subsection 4.2).

All bundle block adjustments are performed using the photogrammetric program system ORIENT/ORPHEUS (Kager et al., 2002). The parameters presented in the following thus refer to the respective definitions.

#### 4.1 Separate Calibration of the Interior Orientation

The calibration of solely the interior orientation makes use of the amplitude data only, and is carried out using a 3-D test field. In order to maximize the number of discernible targets and hence permit precise spatial resections, flat, circular target markers are arranged in regular grids on three pairwise orthogonal planes. During data capture, the camera is guided in a way that the target areas fill the whole image i.e. the distance to the point of intersection of the supporting planes stays approximately the same.

In order to test the short-term reproducibility of the interior orientation and the distortion parameters, 3 image sequences comprising 1000 frames each are captured within an hour. For the purpose of testing the influence of gravity, the optical axis constantly points upwards throughout the first two sequences, while it points downwards in the third one, avoiding rotations

about it in either case. The targets are tracked throughout the sequences using the process described in section 3, see results on Figure 3.

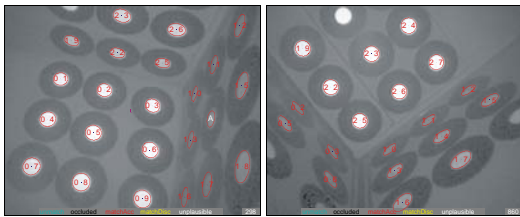


Figure 3. Sample frames of the 1<sup>st</sup> examined image sequence showing the 3-D test field with detected targets.

The image coordinates resulting from target tracking are evaluated in three separate bundle block adjustments where the principal point, the focal length, and affine, tangential, and 3<sup>rd</sup>- and 5<sup>th</sup>-order radial, polynomial distortion parameters are introduced as unknowns. Among the estimated distortion parameters, only the one concerning radial, polynomial distortion of 3<sup>rd</sup> degree deviates significantly from zero, considerably affects the sum of squared residuals, has a relevant influence on the image coordinates and appears to be reproducible. Therefore, the adjustments are repeated with this only term for distortion correction. Figure 4 shows a visualization of its impact, holding the value resulting from the first sequence. As may be inspected on table 1, the principal point results to be largely displaced from the image centre. All three adjustments yield similar values for its x-coordinate, the focal length, and the remaining distortion parameter. However, the principal point's y-coordinate for the third image sequence differs largely from the ones for the first two, suggesting a strong relation to the vertical direction. For the image corners and at an object distance of 7.5m, the maximum variations of the projection centre position given on table 1 yield lateral deviations of object points of 27mm. Taking the whole range of each parameter into account, the effect increases to even 39mm.

Finally, the stability of the interior orientation within a single sequence is investigated. For this purpose, separate interior orientations are introduced for every 100 consecutive frames of the first sequence. The evolution of the resulting principal point locations and focal lengths may also be inspected on Figure 4. The comparison of the fluctuation of the projection centre in the image coordinate system to the prevailing, slightly varying vertical direction during the capture of each set of 100 frames does not discover any relation.

#### 4.2 Integrated Calibration of Interior Orientation and Ranging System

The image sequence gathered for the integrated calibration is intentionally acquired in a way that a widespread domain of capture conditions is covered concerning the object distance, integration time, angle of incidence, and position in the field of view. Large variations of the amplitude follow from these. Substantiated by the experiences described in section 2, the operating time, having awaited the warm-up period, is assumed to have no relevant influence on the measurements, and scattering is not present i.e. the distance between the pixel foot prints and the targets does not affect the range observations. Due to the desired variation of the exterior orientation, the field of control points must be designed differently from the one mentioned in subsection 4.1, taking into account the largely varying image scale and the resulting spread of imaged target

sizes. Hence, the diameter of the target markers increases steadily towards the borders of the test field, allowing images captured close to the board to be oriented using the smaller, central markers, and images of smaller scales to rely on the outer, larger targets. Furthermore, the plane supporting the markers is chosen to be rather highly reflective in the near-infrared frequencies, which allows for shorter integration times and larger object distances and angles of incidence while avoiding the influence of motion blur to the largest extent. Due to restrictions of the software used for data capture, a limited selection of the set of potential integration times, but still a wide range is covered. The resulting sequence comprises 3000 frames for the integration time of 4×4.2ms and 1000 frames for each of the integration times 4×2.2ms, 4×10.2ms, and 4×20.2ms. The calibration data thus comprises 6000 frames, wherefrom the amplitude data again is used for the tracking of targets, as described in section 3. See two samples of the tracking result in Figure 5.

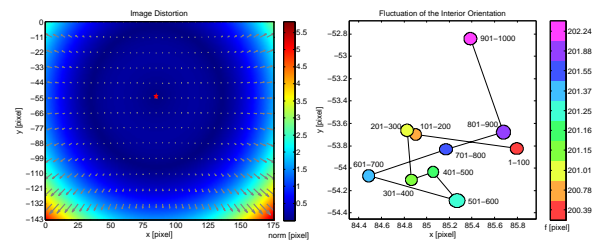


Figure 4. Results from the first image sequence. Left: mean image distortion; its norm as colour coding, arrows pointing from distorted to according undistorted positions (3x enlarged). Right: interior orientations, determined for every 100 consecutive frames. The ranges of corresponding frame numbers are given beneath the error ellipses of the resulting principal point positions. The focal length is colour coded.

[pixel]	sequence 1	sequence 2	sequence 3
$x_0 \pm \sigma_{x_0}$	$85.175 \pm .026$	$84.840 \pm .027$	$84.785 \pm .024$
$y_0 \pm \sigma_{y_0}$	$-53.937 \pm .030$	$-53.728 \pm .029$	$-54.992 \pm .022$
$f \pm \sigma_f$	$201.018 \pm .030$	$200.535 \pm .035$	$200.803 \pm .037$
$a_3 \pm \sigma_{a_3}$	$-0.425 \pm .001$	$-0.435 \pm .001$	$-0.433 \pm .001$

Table 1. Interior orientations and parameter values of radial, polynomial distortion of 3<sup>rd</sup> degree, adjusted for the three investigated image sequences.

Again, the image coordinates obtained from target tracking are introduced into bundle block adjustments, where the interior orientation and the accepted distortion parameter are treated as unknowns. Due to the large number of frames, the sequence is divided into blocks comprising 1000 frames each, yielding adjustments of data with common integration times. The resulting parameter values of the interior orientation and the radial distortion may be inspected on table 2. Despite the worse configuration following from the planarity of the test field, the estimated standard deviations are comparable to those presented on table 1. As the signal level generally grows with the integration time and the image noise accordingly decreases, one may expect an effect of the integration time on the precision of the given parameters. However, this cannot be verified.

Using the parameters on table 2 in combination with the exterior orientations that likewise result from the bundle block adjustments, the projection ray of each pixel is intersected with the known plane of the whiteboard, providing a reference value for the actual range observation. As already mentioned, observations that point to target markers are disregarded.

Measurements in the vicinity and outside the edges of the whiteboard are likewise omitted. Figure 6 presents the distributions of all distance residuals of the examined image sequence, grouped by the integration time they were captured with. Obviously, they all exhibit a negative offset from zero in the range of centimetres.

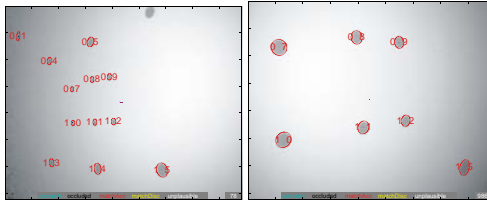


Figure 5. Sample frames from the image sequence used for the integrated calibration of both the interior orientation and the ranging system, with detected targets indicated in red.

[pixel]	1: 4×4.2ms	2: 4×4.2ms	3: 4×4.2ms
$x_0 \pm \sigma_{x_0}$	$84.298 \pm .041$	$84.700 \pm .028$	$85.327 \pm .047$
$y_0 \pm \sigma_{y_0}$	$-54.404 \pm .033$	$-54.500 \pm .030$	$-54.357 \pm .050$
$f \pm \sigma_f$	$200.459 \pm .031$	$200.743 \pm .035$	$200.884 \pm .048$
$a_3 \pm \sigma_{a_3}$	$-0.382 \pm .001$	$-0.386 \pm .001$	$-0.373 \pm .001$
	4: 4×2.2ms	5: 4×10.2ms	6: 4×20.2ms
$x_0 \pm \sigma_{x_0}$	$84.695 \pm .039$	$84.653 \pm .039$	$84.860 \pm .038$
$y_0 \pm \sigma_{y_0}$	$-54.521 \pm .043$	$-54.202 \pm .037$	$-54.631 \pm .036$
$f \pm \sigma_f$	$200.740 \pm .035$	$200.656 \pm .042$	$200.935 \pm .040$
$a_3 \pm \sigma_{a_3}$	$-0.387 \pm .001$	$-0.389 \pm .001$	$-0.378 \pm .001$

Table 2. Interior orientation and radial distortion parameter, adjusted for groups of 1000 frames featuring uniform integration times that are indicated in the table header.

Due to the limited extents of the used whiteboard, the whole distance measurement range cannot be covered. Nevertheless, the confrontation of the residuals with their reference values reveals parts of the periodic non-linearities reported in literature. See Figure 7 for details, bearing in mind that mean residuals for reference values above 2.5m are weakly determined.

The comparison of residuals to the corresponding amplitude observations discovers a very clear relation, supported by an almost equal distribution of residuals over the encoding range. While range measurements with amplitudes above  $2 \times 10^4$  do not appear to be sensitive to changes in the signal strength, there is a very strong effect on values below, see Figure 8.

Examining the influence of the angle of incidence on the residuals does not provide much information. The seeming strong relation above 75gon is supported by few residuals only, see Figure 9.

As a consequence of using only a subset of the range observations, the utilised residuals are not equally distributed on the sensor, which may be verified on Figure 10. Still, each pixel is related to at least 4000 residuals, which gives significance to their mean: with respect to the distances derived from the exterior orientation, the range observations are generally too large, still getting worse towards the principal point, roughly.

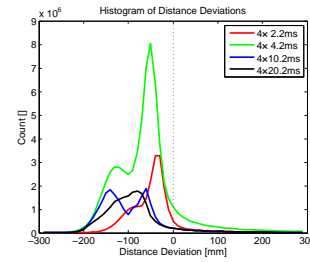


Figure 6. Distribution of distance deviations, grouped by integration time.

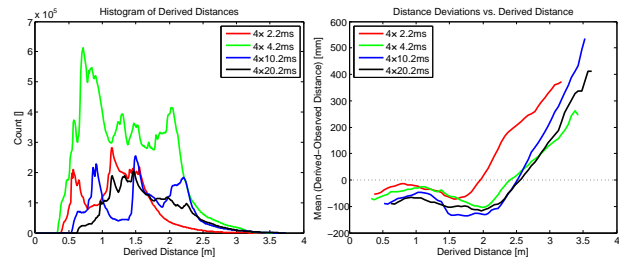


Figure 7. Histogram of derived distances and residuals confronted with them.

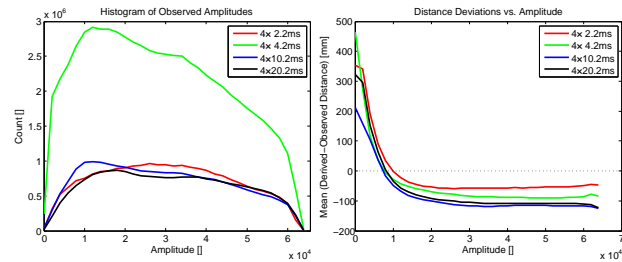


Figure 8. Histogram of observed amplitudes and their relation to range residuals.

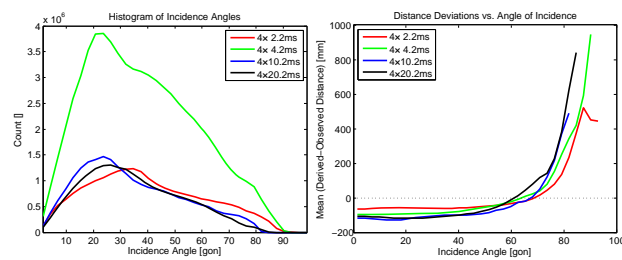


Figure 9. Histogram of incidence angles and their confrontation with ranging residuals.

Figure 11 presents the distribution of pixel footprints on the whiteboard. The precisely circular holes prove the high quality of target centroiding. As large-scale images have mainly been captured in the centre, the density of residuals decreases towards the borders of the test field. For that reason, the apparent effect of radially increasing mean residuals is rather little supported. The absence of scattering is proved again, as there are no circular structures around the voids of the target areas.

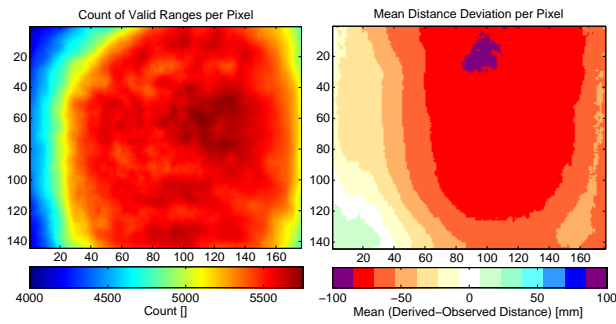


Figure 10: Left: distribution of distance residuals among the sensor pixels, due to omission of measurements on targets and outside the whiteboard not uniform. Right: the mean of all evaluated residuals with respect to each pixel.

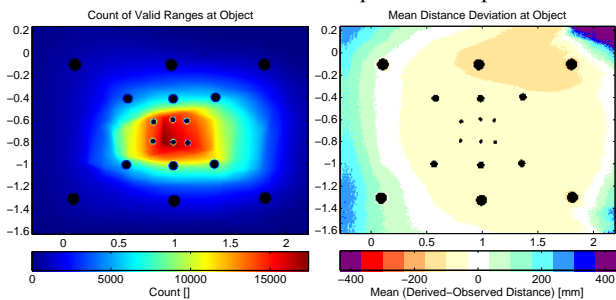


Figure 11: Count (left) and mean (right) of residuals with respect to the location of the corresponding footprints on the whiteboard.

## 5. CONCLUSIONS

Making use of the high temporal resolution of PMD cameras has shown to be advantageous when aiming at their calibration, providing the opportunity to track features and gain high precision and redundancy without manual interaction. Using a single data set that is contaminated by a variety of error sources potentially leads to a better understanding of their interdependencies. Calibrating data gathered under more and more natural conditions, PMD cameras may find their way to quality-oriented applications.

## REFERENCES

Aull, B. F., Loomis, A. H., Young, D. J., Heinrichs, R. M., Felton, B. J., Daniels, P. J. and Launders, D. J., 2002. Geiger-mode avalanche photodiodes for three-dimensional imaging. *Lincoln Laboratory Journal* 13(2), pp. 335–350.

Büttgen, B., Oggier, T., Lehmann, M., Kaufmann, R. and Lustenberger, F., 2005. CCD/CMOS lock-in pixel for range imaging: Challenges, limitations and state-of-the-art. In: H. Ingensand and T. Kahlmann (eds), *1<sup>st</sup> Range Imaging Research Day*, ETH Zurich, Zurich, Switzerland, pp. 21–32.

Elkhalili, O., Schrey, O. M., Mengel, P., Petermann, M., Brockherde, W. and Hosticka, B. J., 2004. A 4x64 pixel CMOS image sensor for 3-d measurement applications. *IEEE Journal of Solid-State Circuits* 39(7), pp. 1208–1212.

Kager, H., Rottensteiner, F., Kerschner, M. and Stadler, P., 2002. ORPHEUS 3.2.1 User Manual. Institute of

Photogrammetry and Remote Sensing, Vienna University of Technology, Austria.

Kahlmann, T., 2007. Range imaging metrology: investigation, calibration and development. PhD thesis, ETH Zurich, Zurich, Switzerland.

Kahlmann, T., Remondino, F. and Ingensand, H., 2006. Calibration for increased accuracy of the range imaging camera Swissranger. *International Archives of the Photogrammetry, Remote Sensing, and Geoinformation Sciences* XXXVI(5), pp. 136–141.

Karel, W., Dorninger, P. and Pfeifer, N., 2007. In situ determination of range camera quality parameters by segmentation. In: A. Grün and H. Kahmen (eds), *Optical 3-D Measurement Techniques VIII*, Vol. 1, ETH Zurich, Zurich, Switzerland, pp. 109–116.

Lange, R., Seitz, P., Biber, A. and Schwarte, R., 1999. Time-of-flight range imaging with a custom solid state image sensor. In: H. J. Tiziani and P. K. Rastogi (eds), *Laser Metrology and Inspection*, Vol. 3823, SPIE, pp. 180–191.

Lindner, M. and Kolb, A., 2006. Lateral and depth calibration of PMD distance sensors. In: *Advances in Visual Computing, Lecture Notes in Computer Science*, Vol. 4292/2006, Springer, pp. 524–533.

Lindner, M. and Kolb, A., 2007. Calibration of the intensity-related distance error of the PMD TOF-camera. In: D. P. Casasent, E. L. Hall and J. Roning (eds), *Intelligent Robots and Computer Vision XXV: Algorithms, Techniques, and Active Vision*, Vol. 6764/1, SPIE, p. 67640W.

Mengel, P., Doemens, G. and Listl, L., 2001. Fast range imaging by CMOS sensor array through multiple double short time integration (MDSI). In: *International Conference on Image Processing*, I.E.E.E.Press, Thessaloniki, Greece, pp. 169–172.

Mure-Dubois, J. and Hügli, H., 2007. Real-time scattering compensation for time-of-flight camera. In: *The 5<sup>th</sup> International Conference on Computer Vision Systems*, Bielefeld, Germany, pp. 117–122.

Niclass, C., Soga, M. and Charbon, E., 2007. 3d imaging based on single-photon detectors. In: A. Grün and H. Kahmen (eds), *Optical 3-D Measurement Techniques VIII*, Vol. 1, ETH Zurich, Zurich, Switzerland, pp. 34–41.

Otepka, J., 2004. Precision target mensuration in vision metrology. PhD thesis, Institute of Photogrammetry and Remote Sensing, Vienna University of Technology, Vienna, Austria.

Pancheri, L., Stoppa, D., Gonzo, L. and Dalla Betta, G.-F., 2007. A CMOS range camera based on single photon avalanche diodes. *tm - Technisches Messen* 74(2), pp. 57–62.

Spirig, T., Marley, M. and Seitz, P., 1997. The multitap lock-in CCD with offset subtraction. *IEEE Transactions on Electron Devices* 44(10), pp. 1643–1647.

Steitz, A. and Pannekamp, J., 2005. Systematic investigation of properties of PMD-sensors. In: H. Ingensand and T. Kahlmann

(eds), *1<sup>st</sup> Range Imaging Research Day*, ETH Zurich, Zurich, Switzerland, pp. 59–69.

Stettner, R., Bailey, H. and Richmond, R. D., 2004. Eye-safe laser radar 3d imaging. In: G. W. Kamerman (ed.), *Laser Radar Technology and Applications IX*, Vol. 5412/1, SPIE, pp. 111–116.

Wallace, A. M., Buller, G. S. and Walker, A. C., 2001. 3d imaging and ranging by time-correlated single photon counting. *Computing & Control Engineering* 12(4), pp. 157–168.

Westfeld, P., 2007. Ansätze zur Kalibrierung des Range-Imaging-Sensors SR-3000 unter simultaner Verwendung von Intensitäts- und Entfernungsbildern. In: T. Luhmann and C. Müller (eds), *Photogrammetrie - Laserscanning - Optische 3D-Messtechnik. Beiträge der Oldenburger 3D-Tage 2007*, Wichmann.

